JACS ARTICLES

Published on Web 09/09/2010

Elliptical Structure of Phospholipid Bilayer Nanodiscs Encapsulated by Scaffold Proteins: Casting the Roles of the Lipids and the Protein

Nicholas Skar-Gislinge,[†] Jens Bæk Simonsen,[†] Kell Mortensen,[†] Robert Feidenhans'l,[‡] Stephen G. Sligar,[¶] Birger Lindberg Møller,[§] Thomas Bjørnholm,[‡] and Lise Arleth*,[†]

Biophysics, Faculty of Life Sciences, Nano Science Center, Faculty of Sciences, and Plant Biology and Biotechnology, Faculty of Life Sciences, University of Copenhagen, DK-1165 Copenhagen, Denmark, and Department of Biochemistry, University of Illinois at Urbana−Champaign, Champaign, Illinois 61820

Received April 12, 2010; E-mail: lia@life.ku.dk

Abstract: Phospholipid bilayers host and support the function of membrane proteins and may be stabilized in disc-like nanostructures, allowing for unprecedented solution studies of the assembly, structure, and function of membrane proteins (Bayburt et al. *Nano Lett.* **2002**, *2*, 853−856). Based on small-angle neutron scattering in combination with variable-temperature studies of synchrotron small-angle X-ray scattering on nanodiscs in solution, we show that the fundamental nanodisc unit, consisting of a lipid bilayer surrounded by amphiphilic scaffold proteins, possesses intrinsically an elliptical shape. The temperature dependence of the curvature of the nanodiscs prepared with two different phospholipid types (DLPC and POPC) shows that it is the scaffold protein that determines the overall elliptical shape and that the nanodiscs become more circular with increasing temperature. Our data also show that the hydrophobic bilayer thickness is, to a large extent, dictated by the scaffolding protein and adjusted to minimize the hydrophobic mismatch between protein and phospholipid. Our conclusions result from a new comprehensive and molecular-based model of the nanodisc structure and the use of this to analyze the experimental scattering profile from nanodiscs. The model paves the way for future detailed structural studies of functional membrane proteins encapsulated in nanodiscs.

Introduction

With the emergence of the field of synthetic biology,[2−5] which combines science and engineering to design and build novel biological functions and systems, it has become increasingly important to identify biological modules that can be assembled into new functional units at the nanoscale. In this context, membrane proteins, being exceptionally advanced nanoscale "machines", constitute a most important group of biomolecules because they carry important functions such as signal transduction, ion pumping, scaffolding, and photosynthetic capabilities. Traditional studies of membrane proteins are based on reconstitution in vesicles or surfactants, and entire pathways may be assembled into a single membrane anchored metabolon.[6,7] Recently, it has furthermore been shown how reconstitution is also possible in so-called nanodiscs.[8−17] Since the size of nanodiscs is compatible with that of typical membrane proteins, nanodiscs hold a very large potential as nanosample environments and allow for a whole new range of

[†] Biophysics, Faculty of Life Sciences, University of Copenhagen.
[‡] Nano Science Center, Faculty of Sciences, University of Copenhagen.
[¶] Department of Biochemistry, University of Illinois at Urbana−Champaign.
[§] Plant Biology and Biotechnology, Faculty of Life Sciences, University of Copenhagen.

(1) Bayburt, T. H.; Grinkova, Y. V.; Sligar, S. G. *Nano Lett.* **2002**, *2*, 853–856.
(2) Purnick, P. E. M.; Weiss, R. *Nat. Rev. Mol. Cell. Bio.* **2009**, *10*, 410–422.
(3) Skerker, J. M.; Lucks, J. B.; Arkin, A. P. *Genome Biol.* **2009**, *10*, 114.
(4) Ghim, C.-M.; Kim, T.; Mitchell, R. J.; Lee, S. K. *Biotechnol. Bioprocess Eng.* **2010**, *15*, 11–21.
(5) Kwok, R. *Nature News* **2010**, *463*, 288–290.
(6) Jorgensen, K.; Rasmussen, A.; Morant, M.; Nielsen, A.; Bjarnholt, N.; Zagrobelny, M.; Bak, S.; Moller, B. L. *Curr. Opin. Plant Biol.* **2005**, *8*, 280–291.
(7) Nielsen, K. A.; Tattersall, D. B.; Jones, P. R.; Moller, B. L. *Phytochemistry* **2008**, *69*, 88–98.
(8) Bayburt, T. H.; Sligar, S. G. *Protein Sci.* **2003**, *12*, 2476–2481.
(9) Civjan, N.; Bayburt, T. H.; Schuler, M.; Sligar, S. G. *Biotechniques* **2003**, *35*, 548–554.
(10) Duan, H.; Civjan, N.; Sligar, S. G.; Schuler, M. *Arch. Biochem. Biophys.* **2004**, *424*, 141–153.
(11) Boldog, T.; Grimme, S.; Li, M.; Sligar, S. G.; Hazelbauer, G. L. *Proc. Natl. Acad. Sci. U.S.A.* **2006**, *103*, 11509–11514.
(12) Leitz, A. J.; Bayburt, T. H.; Barnakov, A.; Springer, B.; Sligar, S. G. *Biotechniques* **2006**, *40*, 601–612.
(13) Nath, A.; Atkins, W. M.; Sligar, S. G. *Biochemistry* **2007**, *46*, 2059–2069.
(14) Whorton, M. R.; Bokoch, M. P.; Rasmussena, S. G. F.; Huang, B.; Zare, R. N.; Kobilka, B.; Sunahara, R. K. *Proc. Natl. Acad. Sci. U.S.A.* **2007**, *104*, 7682–7687.
(15) Banerjee, S.; Huber, T.; Sakmar, T. P. *J. Mol. Biol.* **2008**, *377*, 1067–1081.
(16) Glueck, J. M.; Wittlich, M.; Feuerstein, S.; Hoffmann, S.; Willbold, D.; Koenig, B. W. *J. Am. Chem. Soc.* **2009**, *131*, 12060–12061.
(17) Yao, X. J.; Ruiz, G. V.; Whorton, M. R.; Rasmussena, S. G. F.; Devree, B. T.; Deupi, X.; Sunahara, R. K.; Kobilka, B. *Proc. Natl. Acad. Sci. U.S.A.* **2009**, *106*, 9501–9506.

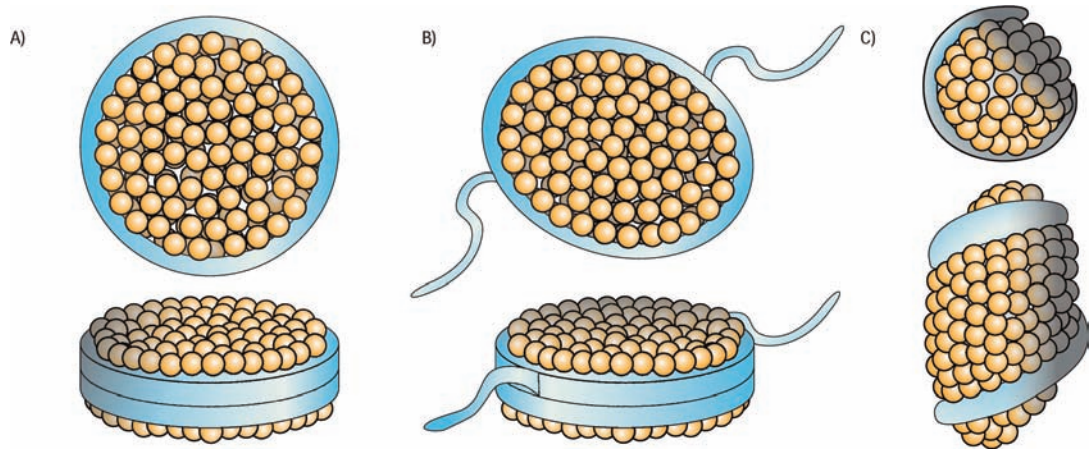

Figure 1. Different suggested nanodisc and HDL model structures, shown from the top and side. (A) Discoidal nanodisc with circular cross section.[24,25,39] (B) Discoidal nanodisc with elliptical cross section and protruding His-tags found in the present study. (C) Double superhelical Apo A1 with a prolate lipid core.[32]

functional and structural studies of membrane proteins in solution and at surfaces.[14,17] Nanodiscs are hence emerging as a versatile system for new fundamental studies of membrane proteins[18] and as potential new building blocks for chemical assembly of new supramolecular synthetic biological nanosystems and entire pathways. Following the original investigations of high density lipoproteins (HDLs),[19−22] the term "nanodisc" was coined by Sligar et al. in this millennium to underscore the possibility to exploit genetic engineering to synthesize and tailor-make such nanoscale objects.[1,23] Structural studies of the nanodiscs comprise small-angle X-ray (SAXS) and neutron scattering (SANS),[24−27] NMR,[16,28,29] atomic force microscopy,[1,30] and electron microscopy.[22,31] Based on these data, the current consensus—still under debate, however[32,33]—is that nanodiscs consists of a phospholipid bilayer surrounded by two amphipatic proteins both encircling the interior bilayer and resulting in a circular disc-like structure (Figure 1). The driving force for the assembly of the unit is the amphiphilic nature of the protein, favoring hydrophobic interactions between the inside of the protein and the alkyl chains of the phospholipid bilayer, resulting in an essentially all-hydrophilic surface exposed to the aqueous environment.[27] Depending on the structure of the phospholipid, the phospholipid bilayer is composed of 120−160 molecules. The current debate[32,33] about the different folding motifs of the amphipatic protein indicates, however, that structural methods so far are not good enough to unambiguously address the detailed structure of neither native HDL particles or engineered APO-A1-based systems including the nanodiscs. This in turn provides a serious obstacle for exploiting the nanodisc systems as a carrier of functional membrane proteins and as a platform to facilitate solution-based structural studies of them.

This has prompted us to embark on a comprehensive experimental and modeling study using SAXS from the native nanodiscs with the goal to enable SAXS and its sister technique, small-angle neutron scattering (SANS), to more routinely provide sufficiently accurate structural information to reveal structural details of membrane proteins embedded in the nanodiscs. In the following we show how a model that properly takes into account the contributions from the amphiphilic protein and from the hydrophobic and hydrophilic parts of the phospholipids provides new insights and improved structural accuracy. This study documents a pronounced elliptical shape of the nanodiscs not previously reported for fully loaded nanodiscs. The so-called twisted-belt model[33] is the only one suggested in the literature that allows an elliptical shape. Contrary to previous models used to analyze SAXS data from nanodiscs, our model design is completely based on the use of the molecular constituents as explicit building blocks of the nanodiscs. This implies that molecular constraints imposed by the phospholipids and the membrane scaffolding protein (MSP) belts, such as partial specific molecular volumes, molecular scattering lengths, and macroscopic sample concentrations, are implicit in the model. Thus, despite the relatively complex structure and potentially large structural parameter space, the theoretical solutions to the model fitting problem are automatically constrained to the much smaller parameter space which is spanned by the physically realistic structures. A similar approach

(18) Borch, J.; Hamann, T. *Biol. Chem.* **2009**, *390*, 805–814.
(19) Matz, C.; Jonas, A. *J. Biol. Chem.* **1982**, *257*, 4535–4540.
(20) Jonas, A. *Methods Enzymol.* **1986**, *128*, 553–582.
(21) Atkinson, D.; Smith, H.; Dickson, J.; Austin, J. *Eur. J. Biochem.* **1976**, *64*, 541–547.
(22) Forte, T.; Nichols, A.; Gong, E.; Lux, S.; Levy, R. *Biochim. Biophys. Acta: Biomembranes* **1971**, *248*, 381–386.
(23) Service, R. *Science* **2004**, *304*, 674–674.
(24) Nakano, M.; Fukuda, M.; Kudo, T.; Miyazaki, M.; Wada, Y.; Matsuzaki, N.; Endo, H.; Handa, T. *J. Am. Chem. Soc.* **2009**, *131*, 8308–8312.
(25) Denisov, I. G.; Grinkova, Y. V.; Lazarides, A.; Sligar, S. G. *J. Am. Chem. Soc.* **2004**, *126*, 3477–3487.
(26) Denisov, I. G.; McLean, M.; Shaw, A.; Grinkova, Y. V.; Sligar, S. G. *J. Phys. Chem. B* **2005**, *109*, 15580–15588.
(27) Shih, A. Y.; Freddolino, P. L.; Sligar, S. G.; Schulten, K. *Nano Lett.* **2007**, *7*, 1692–1696.
(28) Li, Y.; Kijac, A. Z.; Sligar, S. G.; Rienstra, C. M. *Biophys. J.* **2006**, *91*, 3819–3828.
(29) Gu, F.; Jones, M. K.; Chen, J.; Patterson, J. C.; Catte, A.; Jerome, W. G.; Li, L.; Segrest, J. P. *J. Biol. Chem.* **2010**, *285*, 4652–4665.
(30) Blanchette, C. D.; Cappuccio, J. A.; Kuhn, E. A.; Segelke, B. W.; Benner, W. H.; Chromy, B. A.; Coleman, M. A.; Bench, G.; Hoeprich, P. D.; Sulchek, T. A. *Biochim. Biophys. Acta: Biomembranes* **2009**, *1788*, 724–731.
(31) Ye, F.; Hu, G.; Taylor, D.; Ratnikov, B.; Bobkov, A. A.; Mclean, M. A.; Sligar, S. G.; Taylor, K. A.; Ginsberg, M. H. *J. Cell Biol.* **2010**, *188*, 157–173.
(32) Wu, Z.; Gogonea, V.; Lee, X.; Wagner, M. A.; Li, X.-M.; Huang, Y.; Undurti, A.; May, R. P.; Haertlein, M.; Moulin, M.; Gutsche, I.; Zaccai, G.; Didonato, J. A.; Hazen, S. L. *J. Biol. Chem.* **2009**, *284*, 36605–36619.
(33) Thomas, M.; Bhat, S.; Sorci-Thomas, M. *J. Lipid Res.* **2008**, *49*, 1875–1883.

has been applied previously by some of us for simpler self-assembling systems.[34,35]

To identify the roles of the phospholipids and the MSPs in the nanodiscs and to test the accuracy of the model, two different lipid systems were studied and compared. The first, dilaurylphosphatidyl choline (DLPC), has a secondary melting transition and therefore a relatively large intrinsic thermal expansion of the area per headgroup between 0 and 20 °C,[36,37] whereas the second, palmityloleylphosphatidyl choline (POPC), is in the fluid phase throughout the studied temperature range.[38] This gives it a constant and weak intrinsic expansion of its area per headgroup. Our temperature studies of these two nanodisc systems reveal a close agreement with the intrinsic thermal behavior of the lipids, in terms of both the overall expansion of the partial specific volumes of the lipids and the specific expansion of the area per headgroup. However, when confined in the discs, the DLPC is more laterally compressed and POPC is more laterally expanded than in large bilayer liposomes. Our data furthermore suggest that the MSP has an intrinsic tendency to form elliptically shaped discs. The shape of these discs is apparently determined by the temperature.

On the basis of our study we propose that, once the nanodisc is formed, the roles of the lipids and proteins are cast as follows: At any given temperature, the MSP determines the overall elliptical shape of the nanodisc and expands or compresses the area per headgroup of the phospholipids to minimize the hydrophobic mismatch between the bilayer alkyl chains and the hydrophobic inside of the MSPs. The MSP furthermore has sufficient flexibility to slightly adapt the circumference of the nanodiscs such that the lipids in the bilayer leaflet can expand laterally as a response to their intrinsic properties. While our findings are in good qualitative agreement with the consensus model for nanodiscs,[25,26,39] our proposed models are in contrast to the consensus model in that we suggest that maximally loaded nanodiscs do not necessarily have a circular cross section.

Theory and Mathematical Modeling

Our approach for modeling the nanodiscs takes a previously proposed model as its starting point.[25] However, the consequent use of molecular constraints in our approach allows for a much more detailed description than previously obtained. In general, the small-angle scattering intensity of a dilute isotropic suspension of particles can be expressed by

$$I(q) = nb^2P(q) \tag{1}$$

where n is the particle number density and b is the particle excess scattering length, which may also be expressed by $b = V\Delta\rho$. V is the single-particle volume, and $\Delta\rho$ is the average excess scattering length density of the particle as compared to the solvent. $P(q)$, the single-particle form factor intensity, is normalized such that $P(0) = 1$.

For the modeling, we describe the nanodiscs as elliptical discs, with a hydrophobic core region composed of the alkyl chains of the phospholipid bilayer sandwiched between the two hydrophilic

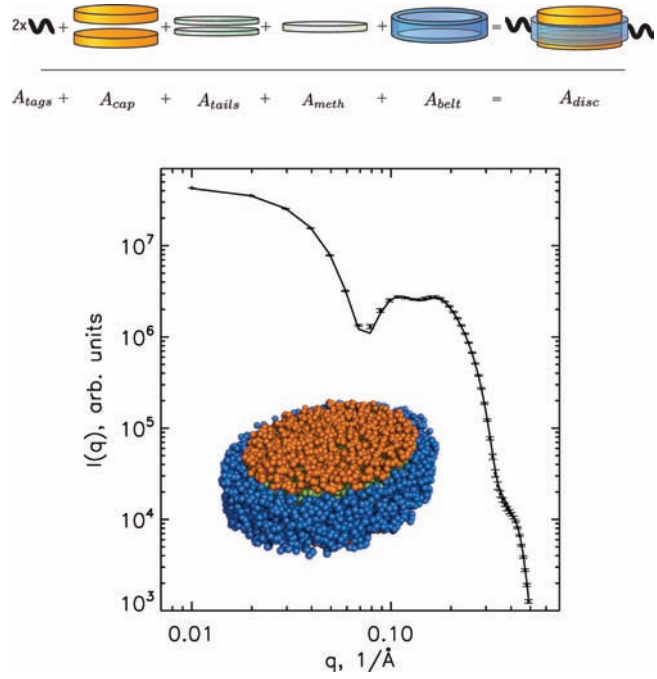

Figure 2. Top: Diagram of the principle for calculating the form factor amplitude of the His-tagged nanodiscs. Bottom: Comparison of the analytical expression for the form factor intensity as calculated from the direct-space model (shown) of the nanodisc structure (points) and from the analytical expression (full line).

headgroup regions. The hydrophilic headgroup regions are composed of the phosphatidyl choline headgroups and hydration water. In agreement with previous models for phospholipid bilayers and nanodiscs, the hydrophobic interior is separated into a central low-density methyl group region, sandwiched between two higher density leaflets composed of the $(CH_2)_n$ chains. The interior phospholipid disc is stabilized by a surrounding belt formed by the two amphiphilic MSPs. The MSP1D1 used in this experiment furthermore features a poly-histidine tag linked to the N-terminal region via a TEV cleavage site. In the following we refer to this 22 amino acid sequence as the His-tag. In the model we assume that this His-tag is protruding out from the belt and that we can describe it as a flexible chain in Gaussian random coil conformation (see Figure 2). Two coils are attached, one for each MSP belt. As the two His-tags have an unknown orientation with respect to each other, we have chosen to place the coils randomly along the rim of the hollow cylinder describing the MSPs.

The model form factor from the nanodiscs is constructed using the approach illustrated in Figure 2 and via the analytical form factor amplitude, $A_{disc}(a,b,h)$, of a short elliptical cylinder of height h and cross-sectional minor and major axes, a and b, as the basic building block.[40]

The short cylinder/disc form factor amplitude, $A_{disc}(a,b,h)$, is normalized such that $|A_{disc}(0)| = 1$. The normalized form factor amplitude of the entire disc (without His-tags) then becomes

$$A_{nanodisc}(q,\phi,\alpha) = (\Delta\rho_{belt}V_{belt}A_{belt} + \Delta\rho_{meth}V_{meth}A_{meth} + \Delta\rho_{tails}V_{tails}A_{tails} + \Delta V_{cap}\rho_{cap}A_{cap})/(\Delta\rho_{belt}V_{belt} + \Delta\rho_{meth}V_{meth} + \Delta\rho_{tails}V_{tails} + \Delta V_{cap}\rho_{cap}) \tag{2}$$

where the $\Delta\rho_i$ values denote the excess scattering length densities of the different constituents, respectively, and the V_i values denote

(34) Arleth, L.; Posselt, D.; Gazeau, D.; Larpent, C.; Zemb, T.; Mortensen, K.; Pedersen, J. S. *Langmuir* **1997**, *13*, 1887–1896.
(35) Arleth, L.; Ashok, B.; Onyuksel, H.; Thiyagarajan, P.; Jacob, J.; Hjelm, R. *Langmuir* **2005**, *21*, 3279–3290.
(36) Finegold, L.; Shaw, W.; Singer, M. *Chem. Phys. Lipids* **1990**, *53*, 177–184.
(37) Tada, K.; Goto, M.; Tamai, N.; Matsuki, H.; Kaneshina, S. *Chem. Phys. Lipids* **2008**, *153*, 138–143.
(38) Jimenez-Monreal, A.; Villalain, J.; Aranda, F.; Gomez-Fernandez, J. *Biochim. Biophys. Acta: Biomembranes* **1998**, *1373*, 209–219.
(39) Shih, A. Y.; Denisov, I. G.; Phillips, J.; Sligar, S. G.; Schulten, K. *Biophys. J.* **2005**, *88*, 548–556.
(40) Pedersen, J. S. Modelling of Small-Angle Scattering from Colloids and Polymer Systems. In *Neutrons, X-rays and Light: Scattering Methods Applied to Soft Condensed Matter*; Linder, P., Zemb, T., Eds.; Elsevier Science B.V.: Amsterdam, 2002; Chapter 16.

the volumes of the different building blocks as outlined in detail in the following section.

The different amplitude terms in eq 2 are derived using the standard approach.[40] As an example, the elliptical hollow cylinder, representing the MSP belt in eq 2, is given by the difference between the form factor amplitudes of two cylinders with different radii and axis ratios of the minor and major axes, a_i and b_i, but the same belt height h:

$$A_{\text{belt}} = A_{\text{disc}}(q, a_{\text{outer}}, b_{\text{outer}}, h) - A_{\text{disc}}(q, a_{\text{inner}}, b_{\text{inner}}, h) \quad (3)$$

The total nanodisc form factor amplitude in eq 2 is absolute squared and orientally averaged to yield the form factor intensity, $P(q)$, using the standard procedure.[40]

As indicated in Figure 2, the model is refined further by incorporating the His-tags described as flexible chains with Gaussian statistics. The final analytical form factor is derived following the same principles as outlined in refs 35, 41, and 42.

In order to independently verify the Fortran implementation of the relatively long and complex equations for the analytical form factor, we compared the outcome of the analytical form factor calculations for a given set of parameters to the small-angle scattering that would be obtained for a geometrical, direct-space model with exactly the same parameters. This small-angle scattering from the direct-space model was calculated as described in ref 43. The direct-space models, along with the corresponding small-angle scattering, calculated via these two different approaches are plotted and compared in Figure 2, and we observe a perfect agreement between the two.

Incorporation of Molecular Constraints. The mathematical model outlined in the previous section is described by a large number of fitting parameters. In order to reduce the degrees of freedom in the model and hence the number of free fitting parameters, we systematically incorporate molecular constraints in the model following the same principles as outlined in ref 34. As a part of this, we exploit the known sample concentration to analyze the data on an absolute scale.

Stoichiometry of the Nanodiscs. Each nanodisc is composed of two MSP belts (the MSP1D1s) and N phospholipids.[1,25] N is a fit parameter in the model, and due to the extremely low critical micellar concentration of the two phospholipids,[44] it is reasonable to assume that the stoichiometry remains constant once the nanodiscs are formed. Consequently, we use the same constant stoichiometry throughout the temperature scans.

Phospholipid Core. Our approach for modeling the phospholipid core is similar in spirit to the models used in the recent structural work on phospholipid bilayers.[45,46] However, we have chosen to use box models instead of Gaussians to model the scattering length density profile. For the modeling, the interior phospholipid bilayer of the nanodiscs is assumed to be separated into a hydrophilic headgroup region and a hydrophobic tail region. The hydrophobic tail region is further divided into a central electron-poor methyl group layer sandwiched between two hydrocarbon-chain-containing layers. The scattering lengths of these three parts of the molecule are determined from the molecular structure and partial specific volumes of the phospholipids.

Initially, we estimate the partial specific molecular volumes of POPC and DLPC to be $\nu_{\text{POPC}} = 1246$ Å^3 and $\nu_{\text{DLPC}} = 985$ Å^3. These values are determined from our densitometry measurements of MSP-free phospholipids in water taken at 20°C. (See further details in Supporting Information.) For the hydrophilic headgroups, a volume of $\nu_{\text{head}} = 319$ Å^3 is used,[47] and for the two methyl groups, a total volume of $\nu_{\text{methyl}} = 108.6$ Å^3 is used,[48] such that the volume of the hydrophobic tails becomes $\nu_{\text{pc}} - \nu_{\text{head}} - \nu_{\text{methyl}}$.

The model furthermore allows for including hydration water in the headgroup region, and we have the number of water molecules per PC headgroup, N_{w}, as an explicit fit parameter.

The fitted area per headgroup, A_{head}, combined with the determined molecular volume of the phospholipids and the fitted hydration number, N_{w}, fixes the total height of the phospholipids including the hydrophobic and hydrophilic heights. The total area of the disc is determined by the stoichiometry N. This area, combined with the fitted axis ratio ε, allows for determining the minor and major axes of the cross section of the lipid core; i.e., the lipid core is modeled with N, N_{w}, ε, and A_{head} as the only free parameters.

Membrane Scaffolding Protein Belt. The MSP1D1 consists of 211 amino acids. For the modeling we assume that 22 of these constitute an intrinsically unfolded His-tag and the remaining 189 constitute the belt, which is mainly folded into α-helical coils.[1]

The total scattering length of the MSP1D1 belt, b_{belt}, is proportional to the number of electrons in the belt via the Thompson scattering length. The number of electrons is counted from the amino acid composition of the MSP1D1. The molecular volume of the MSP1D1, ν_{belt}, is calculated using an average value for the partial specific mass density of proteins of 1.35 cm^3/g.[49] The scattering length density of the protein is then $b_{\text{belt}}/\nu_{\text{belt}}$. The inner minor and major axes are equal to those of the phospholipid core, so the only additional parameters required to describe the belt are the belt height, h_{belt}, and the radius of gyration, R_{g}, of the His-tag.

Resulting Model Fit Parameters. As a result of the molecular constraints, the resulting effective fit parameters are the number of phospholipids per nanodisc, N; the phospholipid area per headgroup, A_{head}; the axis ratio of the phospholipid disc, ε; the number of hydration water molecules, N_{w}; the height of the MSP belt, h_{belt}; and the radius of gyration of the His-tag, R_{g}. In addition to these six primary fit parameters, an effective Gaussian-type roughness term was included to account for the fact that the interfaces between the different constituents of the discs are not infinitely smooth. This term was included by multiplying the total form factor amplitude by $\exp(-(qS_{\text{R}})^2/2)$, where S_{R} is the surface roughness.

Three adjustment parameters were furthermore introduced: a small constant background to be added or subtracted from the data (this parameter should end up close to zero) and (2) scale factors for the partial specific volumes of, respectively, the MSP belt and the phospholipids. These two scale factors should be very close to unity and will account for small differences between the a priori estimated values and the actual values in the nanodiscs in a self-consistent molecular constrained way.

It should be emphasized that we, throughout the mathematical modeling process, have been very cautious to not include more fit parameters than necessary to obtain good and realistic model fits.

Results and Discussion

Initial Data Treatment and Visual Inspection. Figure 3 plots the experimental small-angle scattering from aqueous solutions of nanodiscs made from POPC and DLPC. The two sets of scattering data each have their characteristic features but share an overall behavior with an initial minimum at 0.05−0.07 1/Å followed by a broad peak. This characteristic scattering intensity is due to the complex scattering contrast situation in the

(41) Pedersen, J. S.; Gerstenberg, M. *Macromolecules* **1996**, *29*, 1363–1365.
(42) Pedersen, J. S. *J. Appl. Crystallogr.* **2000**, *33*, 637–640.
(43) Hansen, S. L. *J. Appl. Crystallogr.* **1990**, *23*, 344–346.
(44) Israelachvili, J. N. *Intermolecular and Surface Forces*; Academic Press: London, 1991.
(45) Kucerka, N.; Tristram-Nagle, S.; Nagle, J. F. *J. Membr. Biol.* **2005**, *208*, 193–202.
(46) Nagle, J.; Tristram-Nagle, S. *Biochim. Biophys. Acta: Biomembranes* **2000**, *1469*, 159–195.
(47) Sun, W.; Suter, R.; Knewtson, M.; Worthington, C.; Tristram-Nagle, S.; Zhang, R.; Nagle, J. F. *Phys. Rev. E* **1994**, *49*, 4665–4676.
(48) Tanford, C. *J. Phys. Chem.* **1972**, *76*, 3020–3024.
(49) Mylonas, E.; Svergun, D. I. *J. Appl. Crystallogr.* **2007**, *40*, 245–249.

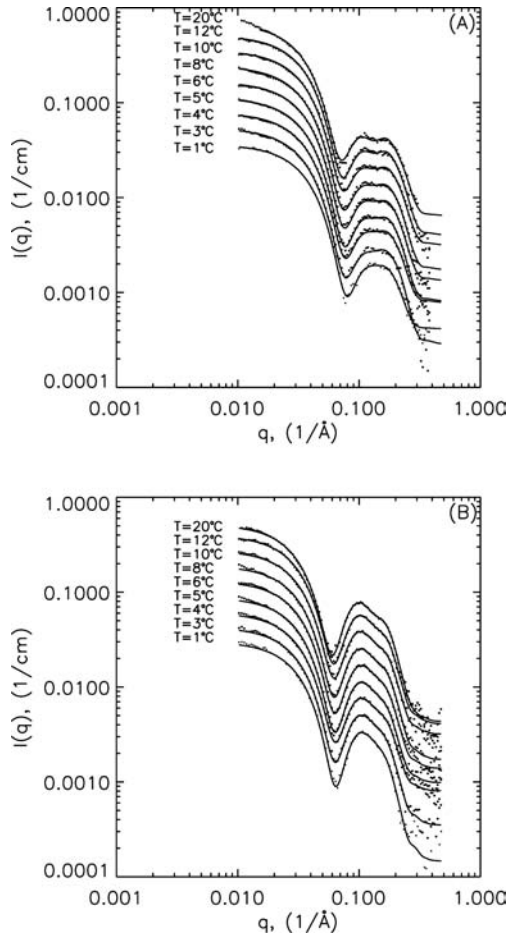

Figure 3. SAXS temperature scans for DLPC nanodiscs (A) and POPC nanodiscs (B). Experimental data points and model fits using the molecular constrained model illustrated in Figure 2. Starting from the lowermost temperature, the data are rescaled by 1.5^n, where n runs from 0 to 8.

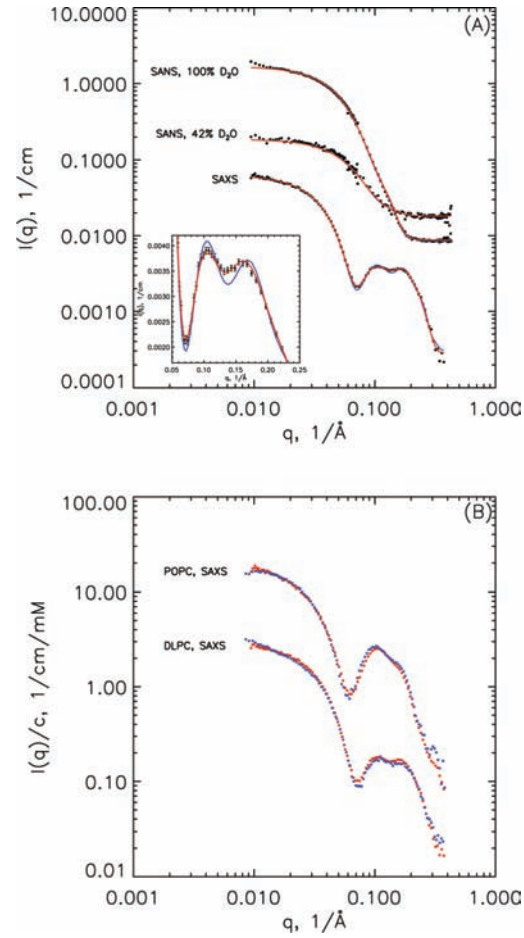

Figure 4. (A) DLPC nanodiscs ($T = 20$°C) measured by SANS and SAXS (black points) and fitted simultaneously with the same structural model for respectively circular (blue) and elliptical (red) nanodiscs. Inset: Zoom-in on the SAXS data with the two model fits. (B) Test of reproducibility of preparation and SAXS measurements of POPC and DLPC nanodiscs. Red points: data measured at Synchrotron SOLEIL. Blue points: data measured at the ESRF synchrotron on a another preparation of the same nanodiscs.

nanodiscs, with negative excess scattering length density for the hydrophobic alkyl chains and positive excess scattering length densities in both the hydrophilic phosphatidyl headgroup regions and the surrounding MSP belt. In both nanodisc systems, the broad peak at 0.1−0.2 1/Å splits into two distinct oscillations as temperature is increased. This shows that the nanodisc structure, including the nanodisc contrast situation, changes with temperature.

Figure 4A plots SAXS and SANS data measured on the same DLPC nanodisc sample. Due to the very different contrast situations for neutrons and X-rays, the same DLPC nanodiscs give rise to very different small-angle scattering curves in the two contrasts, thus emphasizing different features of the nanodisc structure. The DLPC nanodiscs are measured by SANS in the so-called bulk contrast obtained in 100% D_2O, as well as in 42% D_2O/58% H_2O (v/v), where the protein belts and the hydrophilic headgroups are, in practice, matched. These two SANS contrasts complement the SAXS data, which are, on the other hand, very sensitive to the fine balance between the electron-poor hydrophobic regions and the electron-rich hydrophilic regions. The use of three contrasts reduces the number of possible solutions to the model fitting problem significantly, increases the certainty of the structural model, and allows, in practice, for extracting even more detailed information.

In order to investigate the reproducibility of the nanodisc preparations, we measured SAXS data on several preparations of nanodisc samples. Typical examples of data obtained this way are shown in Figure 4B. It is clearly seen that the structure of the nanodiscs formed, as represented in terms of the SAXS data, is very reproducible.

Figure 5 shows examples of real-space representations of the small-angle scattering data in terms of the pair-distance distribution functions, $p(r)$, as determined via indirect Fourier transform of the scattering data.[50,51] The overall similarities between the POPC and DLPC nanodisc systems are obvious. The strong temperature dependence of the SAXS data, now represented in terms of the $p(r)$ functions, is also evident. In both cases, the D_{max} of the $p(r)$, i.e., the maximum dimension of the particles, reaches zero around 120 Å. The maximum dimensions of the nanodiscs formed in the two systems are therefore, as expected, quite similar and in both cases close to 120 Å. Furthermore, both systems exhibit a clearly visible tail starting at ∼100 Å and extending to 120 Å. This is fully consistent with our expectations of how a His-tag connected to the outside of the belt should appear in the $p(r)$ representation. We also observe that the broad peak initially centered around 60 Å splits into two broad peaks as temperature is increased from 1 to 20 °C;

(50) Glatter, O. *J. Appl. Crystallogr.* **1977**, *10*, 415–421.
(51) Pedersen, J. S.; Hansen, S. L.; Bauer, R. *Eur. Biophys. J.* **1994**, *22*, 379–389.

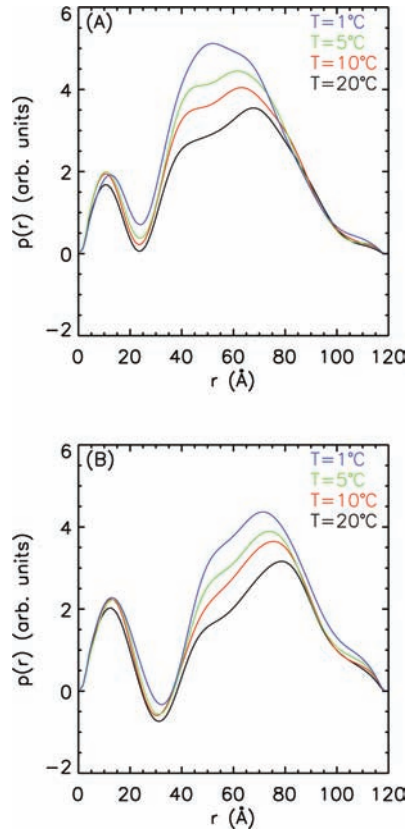

Figure 5. Examples of pair-distance distribution functions determined from the SAXS temperature scans of DLPC nanodiscs (A) and POPC nanodiscs (B).

i.e., the temperature-dependent "peak-splitting" is visible in both direct and reciprocal space. However, the detailed nanodisc structure is far too complex to allow for a model-free interpretation of this behavior based on a pure inspection of the obtained $I(q)$ and $p(r)$ data.

Model Fit Results. a. Testing the Hypotheses of the Structure of the Nanodiscs. So far, there has been consensus in the literature that fully loaded nanodiscs are circular,[14,25,26,39] and most small-angle scattering (SAXS and SANS) data from nanodiscs have been interpreted with this implicit assumption. Hence, the process of analyzing the scattering data in the present project naturally started with a model for circular discs. Using this approach, it was, however, quickly found that the scattering data could not be described satisfactorily. Figure 4A (blue curve) shows an example of a simultaneous fit of the circular model to a set of SANS and SAXS data obtained on the DLPC nanodisc system. While the general fit quality is decent, with a reduced χ^2 of 2.36, some clear and systematic deviations between model and experimental data are clearly observed. Because of the contrast situation, the deviations are most clearly observed in the SAXS data (see inset in Figure 4A), but they are also significant in the SANS data. These systematic deviations are a clear indication that the nanodiscs are either not circular or not monodisperse, or both.

In special cases, small-angle scattering data allow for separating dispersity in size and shape.[52,53] However, the small-angle scattering data obtained on the nanodisc system do not allow for such a separation; the model for monodisperse elliptical nanodiscs already gives perfect simultaneous fits to the SANS and SAXS data on the DLPC nanodiscs. This implies that a more complex model with a higher number of fit parameters cannot be used for extracting more detailed information from the data.

The structure of the MSP and the expected constant length of the MSP speak against a significant polydispersity and suggest that the shape deformation is the leading term. Consequently, the small-angle scattering data were analyzed in terms of a model for shape deformations in terms of elliptical nanodiscs. The red curve in Figure 4A is the best simultaneous fit obtained using this approach. The reduced χ^2 is 1.85, and there are no systematic deviations between model and data. The resulting model-fit parameters are listed in Table 1.

b. Fixing the Stoichiometry of the Nanodiscs. The absolute scaled SANS data (100% D_2O) are very sensitive to the stoichiometry of the nanodiscs, once the sample concentration is known. We have therefore determined the stoichiometry of the DLPC nanodiscs from the above-discussed simultaneous fit. This gives a stoichiometry of 76 DLPCs per MSP, corresponding to $N = 152 \pm 1$. This number lies close to the value obtained for DMPC nanodiscs,[54] and N was fixed to this value throughout the analysis of the DLPC system. For the POPC nanodiscs, the SAXS data were consistent with a stoichiometry of 61.5 POPCs per MSP, i.e., $N = 123 \pm 8$. This value is in good accordance the value of $N = 124 \pm 5$ that has previously been obtained,[1,25] and $N = 124$ was used throughout the analysis of the POPC data.

c. Model Fits to the SAXS Temperature Scans. The model fit results are plotted along with the experimental data in Figure 3. The obtained χ^2 values are all at or below unity, and as seen from the plots, the model fit quality is excellent and the model fits captures all significant features of the data.

The resulting fit parameters as well as deduced structural parameters of the nanodiscs at 1 and 20 °C are listed in Table 1. Furthermore, Figure 6 plots the temperature dependence of (A) the partial specific molecular volume, (B) the area per PC headgroup, (C) the axis ratios of the DLPC and POPC nanodiscs, and (D) the circumference of the MSP belts. All parameters are obtained from the model fits.

The observed partial specific molecular volumes for DLPC and POPC (see Figure 6A) are seen to increase slowly with temperature. This is the case both when determined directly from the densitometry measurements on plain and MSP-free samples of DLPC and POPC (multilamellar vesicle systems) and when determined from the model fits to the nanodisc samples. As clearly seen in the plot, the molecular volumes measured in these two ways are fully proportional to each other. For both DLPC and POPC, the values for partial specific molecular volumes are 2−3% higher in the MSP nanodiscs than in the MSP-free bilayer. With only two data series, it is not possible to tell whether the offset is a systematic result of a slightly different packing of the phospholipids when localized in multilamellar vesicles and nanodiscs, respectively, or whether the offset is simply an unsystematic result of small errors in the determination of the sample concentrations for the densitometry samples. However, in either case, the excellent agreement between the results obtained by these two independent approaches is a very strong proof of the self-consistency of the SAXS data analysis.

(52) Caponetti, E.; Floriano, M.; Didio, E.; Triolo, R. *J. Appl. Crystallogr.* **1993**, *26*, 612–615.
(53) Arleth, L.; Pedersen, J. S. *Phys. Rev. E* **2001**, *63*, 061406.
(54) Bayburt, T. H.; Sligar, S. G. *FEBS Lett.* **2010**, *584*, 1721–1727.

Table 1. Results from the Simultaneous Fits to SANS and SAXS Data on DLPC Nanodiscs at 20 °C (Marked N/X) and from the Fits to the SAXS Temperature Scan on DLPC and POPC Nanodiscs (Marked X) at 20 and 1 °C[a]

	DLPC, N/X	DLPC, X		POPC, X	
	20 °C	20 °C	1 °C	20 °C	1 °C
		Fit Parameters			
N	152 ± 1	152[b]	152[b]	124[b]	124[b]
ε	1.29 ± 0.02	1.26 ± 0.03	1.34 ± 0.04	1.31 ± 0.02	1.39 ± 0.03
A_{head}, Å^2	58.6 ± 0.2	58.8 ± 0.3	52.2 ± 0.3	70.6 ± 0.6	67.4 ± 1.2
N_w	0.0[b]	0.0[b]	0.0[b]	7.2 ± 1.0	13.6 ± 2.0
ν_{PC}, Å^3	997.5 ± 0.4	994.6 ± 0.7	965.8 ± 0.9	1277.3 ± 1.0	1254.5 ± 2.5
ν_{MSP}, Å^3	30217 ± 33	30658 ± 53	30954 ± 65	29851 ± 39	29410 ± 99
H_b, Å	24.0[b]	24.0[b]	24.0[b]	24.0[b]	24.0[b]
R_g, Å	12.7 ± 0.7	12.7[b]	12.7[b]	12.7[b]	12.7[b]
		Deduced Parameters			
H_{total}, Å	34.0 ± 0.1	33.8 ± 0.2	37.0 ± 0.2	42.7 ± 0.9	49.4 ± 1.9
$H_{hydrophobic}$, Å	23.0 ± 0.1	22.8 ± 0.2	24.2 ± 0.3	27.2 ± 0.2	27.7 ± 0.4
A_{disc}, Å^2	4408 ± 13	4428 ± 23	3924 ± 65	4314 ± 39	4193 ± 73
D_{minor}, Å	65.9 ± 0.7	66.9 ± 1.0	61.0 ± 1.6	65.1 ± 0.8	62.0 ± 1.4
D_{major}, Å	85.1 ± 1.4	84.3 ± 2.5	81.9 ± 2.7	85.1 ± 1.5	86.1 ± 2.3
d_{belt}, Å	8.5 ± 0.8	8.7 ± 1.4	9.1 ± 1.5	8.5 ± 0.9	8.5 ± 1.6

[a] Fitting parameters are those determined directly by the fits. Deduced parameters are derived from the fitted parameters as a consequence of the molecular constraints imposed on the model. N, number of phospholipids per nanodisc; ε, axis ratio of lipid core; A_{head}, area of the PC headgroup; N_w, hydration number; ν_{PC} and ν_{MSP}, partial specific molecular volumes of the phospholipid and MSP, respectively; H_b, height of the MSP belt; R_g, radius of gyration of the His-tags; A_{disc}, total area of the phospholipid part of the disc; H_{total}, total height of the phospholipid bilayer; $H_{hydrophobic}$, height of hydrophobic bilayer; D_{minor} and D_{major}, minor and major diameters of the phospholipid bilayer, respectively; and d_{belt}, thickness of the MSP belt. [b] Parameter not fitted.

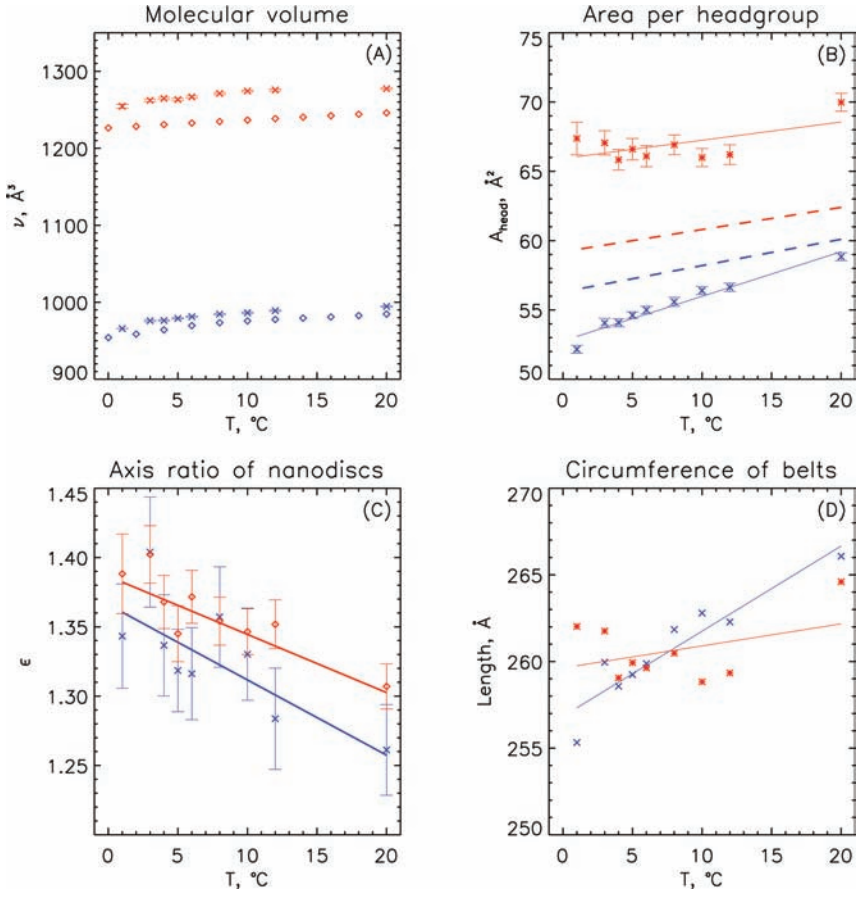

Figure 6. (A) Partial specific molecular volume, ν, plotted as a function of temperature for DLPC (blue) and POPC (red). Diamonds: data obtained from densitometry measurements. Crosses: data obtained from the SAXS analysis. (B) Temperature dependence of the molecular area per phospholipid headgroup. Same colors as in (A). Crosses: values obtained from the SAXS analysis. Full lines: fit of straight lines to the experimental data. Dashed lines: plots of the temperature dependence of the same lipids when localized in large bilayer vesicles. (C) Temperature dependence of the axis ratios of the nanodiscs. Same colors as in (A). Points: data determined from the SAXS analysis. Full lines: fit of straight lines to the experimental data. (D) Temperature dependence of the circumference of the nanodiscs. Same colors as in (A). Points: data determined from the SAXS analysis. Full lines: fit of straight lines to the experimental data.

The observed areas per headgroup of DLPC and POPC when localized in the nanodiscs are plotted in Figure 6B. In both cases, a temperature-dependent expansion is clearly observed. Straight lines fitted to the two sets of data give the following empirical

expressions for the area per headgroup as a function of temperature, T, measured in °C: $A_{\mathrm{DLPC,\,ND}} = (52.8 + 0.32T)$ Å^2 and $A_{\mathrm{POPC,\,ND}} = (65.9 + 0.13T)$ Å^2. It is relevant to compare the temperature-dependent expansion in the nanodiscs to that observed for phospholipids in "free" bilayers. Kucerka and coworkers reported the following temperature dependence:[55,56] $A_{\mathrm{DLPC}} = (56.3 + 0.19T)$Å^2 and $A_{\mathrm{POPC}} = (59.7 + 0.16T)$Å^2 (see plots in Figure 6B). The equations were obtained via simultaneous analysis of SANS and SAXS data on DLPC and POPC bilayers using a fully molecular constrained approach similar in spirit to the one used in the present article.[55] It should be emphasized that the equations were extrapolated from the temperature dependence observed around $T = 30$ °C and are only expected to be valid in the fluid phase, i.e., for $T > \sim 0°$ C in the case of POPC and for $T > \sim 10$ °C in the case of DLPC. It is clearly seen from the plots that DLPC has a smaller area per headgroup in nanodiscs than it has in free bilayers, whereas the POPC behaves oppositely and has a *larger* area per headgroup in nanodiscs than in free bilayers. Regarding the temperature-dependent lateral expansion, it is seen that POPC has a similar expansion of the areas per headgroup in nanodiscs and in "free" bilayers, while DLPC, where the lipids move through a secondary melting transition between 0 and 10 °C,[36,37] has, as expected, on average a larger expansion coefficient in nanodiscs in the studied temperature range than in the "free" bilayer data from the fully fluid phase above this melting transition. The total bilayer areas in the nanodiscs (see Table 1) are in very close agreement with results obtained using atomic force microscopy.[1]

Figure 6C plots the temperature dependence of the axis ratios, ε, of the two types of nanodiscs. In both systems ε decreases significantly with increasing temperature, implying that the discs become more circular with increasing temperature. Interestingly, the data suggest that there is no dependence between lipid type and disc shape; i.e., the larger temperature expansion of the DLPC than of POPC is not reflected in a corresponding larger decrease of the axis ratio.

Figure 6D plots the circumference of the belts as estimated by

$$P = 2\pi\sqrt{\left[(r_{\mathrm{minor}} + d_{\mathrm{belt}})^2 + (r_{\mathrm{major}} + d_{\mathrm{belt}})^2\right]/2}$$

In both systems the perimeter increases with temperature. However, the increase is significantly stronger for the DLPC nanodiscs than for the POPC nanodiscs. The stronger increase of the perimeter of DLPC nanodiscs is consistent with the larger area-expansion in this system in the studied temperature range. Assuming that the 189 amino acids in the belt part of the MSP make a chain of α-helical coils with a helical pitch of 1.5 Å per residue, the maximal extension of the belt becomes ∼284 Å. For both the DLPC and the POPC nanodiscs, the circumference is slightly lower than this value. This indicates that the belt is not fully stretched in the nanodiscs, which leaves some flexibility in the system for adapting to the increasing disc area.

The model fits are not very sensitive to the belt height when it is varied between 20 and 30 Å. Therefore, in the fitting process, it was decided to fix the belt height to 24 Å, which is compatible with the thickness of two α-helical chains. This poorly defined height is most likely a result of our attempt to model the curved α-helical belts with an effective edged hollow cylinder structure. Along this line, it is also relevant to address the questions about the conformation of the MSP belt and whether both belts surround the nanodiscs or they form half-circles or ellipses in a picket-fence-like structure.[13] Unfortunately, our present data do not contain information to answer this question.

The hydrophobic thickness values (see Table 1) are comparable for the DLPC and POPC nanodiscs, and both of them are relatively close to the belt height. At 20 °C we find a hydrophobic bilayer thickness of 24 Å for DLPC and 28 Å for POPC. Both systems show a slightly decreasing thickness for increasing temperature, directly related to the increasing area per headgroup. This finding suggests that the phospholipid bilayer adapts to the MSP belt to minimize the membrane/belt hydrophobic mismatch.[44,57]

The His-tags are clearly observed. They are revealed in the $p(r)$ functions as well as in the reciprocal space SAXS data, and a model term was included to explicitly take them into consideration such that sufficiently good model fits could be obtained. The simultaneous fit (Figure 4) gave a radius of gyration of $R_g = 12.7 \pm 0.7$ Å for the His-tags. No significant deviations from this value were found throughout the two temperature scans, and the final fits were performed with fixed $R_g = 12.7$ Å. This value, which is at the higher end of what we expected, most likely results from a combination of the relatively high rigidity of the His-tag and the low number of effective Kuhn lengths, such that the tag protrudes more or less perpendicular to the belt surface.

As mentioned previously, the number of hydration water molecules per PC headgroup is an explicit fit parameter in the model. When the data from the DLPC nanodiscs were fitted, we obtained, much to our surprise, values for the hydration number very close zero and sometimes even slightly negative. The latter situation is obviously unphysical, and in order to constrain the fits to physically realistic models, the hydration number was fixed to zero for the entire DLPC series. The very low hydration number may be a consequence of the lateral compression of the DLPC when localized in nanodiscs and may even suggest that the DLPC hydration water molecules are more densely packed (i.e., with a lower partial specific molecular volume) than bulk water molecules. However, the present data do not, unfortunately, allow us to investigate this effect in further detail.

In the POPC system we observe a decreasing hydration with increasing temperature. At 1 °C, we find that the POPC headgroups have 14 water molecules per PC headgroup, whereas at 20 °C, each POPC is associated with 7 water molecules. These numbers are in good accordance with the numbers reported in previous work,[45] and the temperature-dependent dehydration of the hydrophilic headgroups is fully consistent with what is observed in many other amphiphilic systems.[58]

General Discussion. The experimental SAXS data obtained from the nanodiscs are fully consistent with a model for elliptical disc-shaped nanodiscs. The SAXS-determined phospholipid partial specific volumes, including their thermal expansions, are in perfect agreement with the results of densitometry measurements and provide an internal self-consistency check of the SAXS analysis. While our observations do not explicitly rule

(55) Kucerka, N.; Nagle, J. F.; Sachs, J. N.; Feller, S. E.; Pencer, J.; Jackson, A.; Katsaras, J. *Biophys. J.* **2008**, *95*, 2356–2367.
(56) Personal communication cited with permission from N. Kucerka, Canadian Neutron Beam Centre, National Research Council of Canada, Chalk River Laboratories, Chalk River, Canada.
(57) Mouritsen, O.; Bloom, M. *Biophys. J.* **1984**, *46*, 141–153.
(58) Strey, R. *Colloid Polym. Sci.* **1994**, *272*, 1005–1019.

out a structure like the double-helical structure recently proposed by Wu and co-workers,[32] we find the elliptical disc model much more realistic because it allows the phospholipids to form a flat bilayer, in accordance with their close-to-unity packing parameter[44,59] and the relatively high bending rigidity of phospholipid bilayers, typically on the order of $10-20\ k_BT$.[44,60] Our finding of an elliptical lipid core is nevertheless in qualitatively good agreement with the results of Wu and co-workers.[32]

a. Elliptical versus Circular Shape of the Nanodiscs. So far, there has been consensus in the literature that nanodiscs are circular when they are fully loaded[14,25,26,39] but become elliptical/deformed when they are less than fully loaded.[39] This consensus follows from an intuitively tempting underlying model with a fixed disc circumference, defined by the MSP, which gives rise to an increasingly circular shape as more and more phospholipids are loaded into the nanodiscs. This underlying model implicitly defines the "fully loaded state" as the state that gives circular nanodiscs.

On this basis, it is natural to question to what extent the nanodiscs studied in the present project have been fully loaded. In the above-discussed intuitive model, our finding of elliptical discs would definitely imply that the discs are not fully loaded. However, the nanodiscs studied in the present work were carefully prepared through protocols that are optimized for maximal loading of the nanodiscs, the sample preparations appear very reproducible, as judged both by the size exclusion chromatograms and in particular by the much more sensitive SAXS analysis (Figure 4B).

Regarding the disc self-assembly from a statistical mechanics point of view, however, it is clear that the fully loaded state with a circular disc and a fully stretched belt is very unlikely. The argument is that there is only one way of loading the disc maximally to M phospholipids per nanodisc, while there will be M ways of loading the disc with $M-1$ phosholipids, $M(M-1)/2!$ ways of loading the disc with $M-2$ phosholipids, and, generally, $M!/N!$ ways of loading the disc with $M-N$ phospholipids. Thus, entropy will always favor the less than fully loaded conformations, and fully loaded discs are possible only in the limit of infinitely strong cooperativity. Another consequence of this line of argument is that, if the cooperativity is very strong, then the system will spontaneously microphase-separate into fully loaded and minimally loaded nanodiscs, such that fully loaded (nearly) circular discs will be formed independently of the initial ratio between phospholipids and belts, and such that optimizing the ratio will optimize the nanodisc yield but not affect the shape of the fully loaded fraction of assembled nanodiscs. This hypothesis lends experimental support to the original results in ref 1 that, by means of a combination of size exclusion chromatography and radioactively labeled phopspholipids, showed that the stoichiometry of the formed nanodiscs depends only weakly on the initial phospholipid-to-MSP ratio.

On the basis of these points and our experimental observations, we propose that, in experimental situations, maximally loaded nanodiscs along with APO-A1 discs will in practice always have an elliptical cross section. We therefore propose that our observation of elliptical nanodiscs is the rule rather than the exception to the rule. We plan to subject this hypothesis to a more careful test in an upcoming study.

b. Implications for Incorporation of Membrane Proteins into Nanodiscs. One of the central findings presented in this work is that the phospholipids localized in nanodiscs are slightly perturbed as compared to when they are localized in bilayer liposomes. We propose that this is driven by the MSP belt and the resulting minimization of the hydrophobic mismatch between the hydrophobic interiors of the MSP belt and the phospholipd bilayer.[57]

As the partial specific molecular volume of the phospholipid is virtually incompressible, the molecular area and hydrophobic height are inversely proportional to each other. Consequently, the molecular area decreases as the hydrophobic height increases as a response to the hydrophobic mismatch minimization and vice versa. For the DLPC, where the hydrophobic height is increased by the MSP, this results in a relatively smaller area per headgroup and also a very small value for the hydration number, which is apparently close to zero. This very small hydration number may affect the lateral packing of the PC headgroups. For the POPC, the hydrophobic height is decreased by the MSP, and this results in a significantly larger area per headgroup, whereas the observed hydration numbers (see Table 1) are comparable to those reported from phospholipid bilayer liposome systems.[45] A consequence of this finding is that the lateral pressure within the phospholipid bilayer environment will be different in nanodiscs and in bilayer liposomes. For DLPC, a higher lateral pressure will be obtained in nanodiscs as compared to in bilayer liposomes, whereas the opposite is the case for POPC.

That the phospholipids in nanodiscs are in a different state compared to bilayer liposomes is also supported by other experimental reports. From DSC measurements, the melting transition temperature of DMPC and DPPC is observed to shift toward higher temperatures,[26] whereas in a SANS study, the activation energy required to move one lipid into solution is decreased in nanodiscs.[24]

This effect may be relevant when using nanodiscs as a platform for investigating transmembrane proteins. It implies a relatively simple mechanism for the interplay between phospholipid type and functioning of the membrane protein and suggests that a detailed study should be conducted where the effect of phospholipid type is directly correlated with the membrane protein function.

Conclusion

A detailed and fully molecular constrained model for the small-angle scattering from nanodisc particles has been derived, and the model has been used to investigate the temperature dependence of DLPC and POPC nanodiscs and to identify the roles of phospholipids and MSP belts in nanodiscs. DLPC and POPC were chosen because they have very different intrinsic expansion coefficients of their areas per headgroup in the studied temperature range from 1 to 20 °C.

The nanodiscs were concluded to have an elliptical shape with the His-tags protruding out from the outer rim of the belts. The shape of the nanodiscs becomes more circular as temperature increases. Despite the different intrinsic expansion coefficients of DLPC and POPC, we do not observe significant differences in the temperature dependence of the shapes in the two systems. However, as a response to the relatively larger expansion of the DLPC, the belt perimeter increases more in the case of DLPC nanodiscs than in the case of POPC discs.

(59) Israelachvili, J. N.; Mitchell, D. J.; Ninham, B. W. *J. Chem. Soc., Faraday Trans. 2* **1976**, *72*, 1525–1568.
(60) Yi, Z.; Nagao, M.; Bossev, D. P. *J. Phys.-Condens. Matter* **2009**, *21*, 155104.

The areas per headgroup of POPC and DLPC in nanodiscs differ significantly from the values observed in liposomes and "free" bilayers. POPC is expanded by the nanodiscs, while DLPC is squeezed. The POPC expansion and the DLPC squeezing drive the hydrophobic thicknesses of both lipids toward the height of the MSP belt. This shows that the phospholipids adapt their hydrophobic bilayer thickness and consequently their areas per headgroup to minimize the hydrophobic mismatch at the protein−lipid interface. This minimization of the hydrophobic mismatch may be the driving force for the effective squeezing of the DLPC and expansion of the POPC.

Altogether, our data and analysis clearly document that it is the protein belt that determines the shape and temperature dependence of the disc.

An important biological consequence of our findings of both the elliptical shape and the temperature dependence of the system is that it shows that the HDL particles are rather flexible particles that may adapt their circumference to increased or decreased load of phospholipids and cholesterol. In applications of nanodiscs as a platform for investigating membrane proteins, our findings suggest that the lateral pressure within the nanodiscs will depend strongly on the chosen phospholipid type. This will most likely feed back on the activity of the inserted membrane proteins. In a wider perspective, our detailed determination of the structure of the nanodiscs is a crucial step on the way to using nanodiscs as a platform for SAXS and SANS determinations of the low-resolution structure of membrane proteins.

Acknowledgment. The authors thank Dr. J. Perez and Dr. G. David at the SWING beamline at SOLEIL, the national French synchrotron facility, and we gratefully acknowledge the access to beamtime at SOLEIL. The authors thank Dr. Y. Cerenius and Dr. T. Plivelic at the I711 beamline at Max-lab, the national Swedish synchrotron facility, and we gratefully acknowledge the access to beamtime for pilot experiments at Max-Lab. The authors thank Dr. A. Round at the ID14-3 Bio-SAXS beamline at ESRF, the European Synchrotron Radiation Facility, and Dr. R. Schweins at the SANS instrument at beamline D11 at ILL, Institute Laue Langevin. We gratefully acknowledge the access to "simultaneous" SAXS and SANS beamtime at ILL and ESRF. The authors also thank Dr. T. Hamann for introducing us to the preparation of nanodiscs, Dr. N. Kucerka for sharing his unpublished results on POPC and DLPC bilayer membranes with us, and Dr. I. Denisov for enlightening discussion during the writing of the manuscript. Finally we thank the Danish Government funded UNIK Synthetic Biology program for co-funding of the project.

Supporting Information Available: Detailed account of the applied procedure for preparing the nanodiscs, report of the densitometry experiments, and experimental report of the SAXS/SANS experiments. This material is available free of charge via the Internet at http://pubs.acs.org.

JA1030613